Fish Population and Behavior Revealed by Instantaneous Continental Shelf-Scale Imaging

Nicholas C. Makris *et al.*

Science **311**, 660 (2006);
DOI: 10.1126/science.1121756

Science (print ISSN 0036-8075; online ISSN 1095-9203) is published weekly, except the last week in December, by the American Association for the Advancement of Science, 1200 New York Avenue NW, Washington, DC 20005.

Fish Population and Behavior Revealed by Instantaneous Continental Shelf–Scale Imaging

Nicholas C. Makris,[1]* Purnima Ratilal,[2] Deanelle T. Symonds,[1] Srinivasan Jagannathan,[1] Sunwoong Lee,[1] Redwood W. Nero[3]

Until now, continental shelf environments have been monitored with highly localized line-transect methods from slow-moving research vessels. These methods significantly undersample fish populations in time and space, leaving an incomplete and ambiguous record of abundance and behavior. We show that fish populations in continental shelf environments can be instantaneously imaged over thousands of square kilometers and continuously monitored by a remote sensing technique in which the ocean acts as an acoustic waveguide. The technique has revealed the instantaneous horizontal structural characteristics and volatile short-term behavior of very large fish shoals, containing tens of millions of fish and stretching for many kilometers.

There is substantial evidence that fish populations are rapidly declining worldwide (*1*, *2*), yet with conventional sea-going survey methods (*3*–*7*) it is difficult to accurately enumerate fish populations (*6*, *8*, *9*) and nearly impossible to study the behavioral dynamics of very large social groups or shoals of fish (*10*), including the impacts of population decline (*11*, *12*). This is because conventional methods rely on highly localized measurements made from slow-moving research vessels, which typically survey along widely spaced line transects to cover the vast areas that fish inhabit, and so greatly undersample the environment in time and space, leaving highly ambiguous records. We assessed fish populations with a remote sensing technology involving ocean acoustic waveguide propagation that surveys at an areal rate that is roughly one million times greater than that of conventional fish-finding methods. The waveguide technology makes it possible to continuously monitor fish population dynamics, behavior, and abundance, with minute-to-minute updates over thousands of square kilometers, producing records without aliasing (*13*, *14*) in time and space.

With the waveguide remote-sensing technology, we observed (i) instantaneous hori-

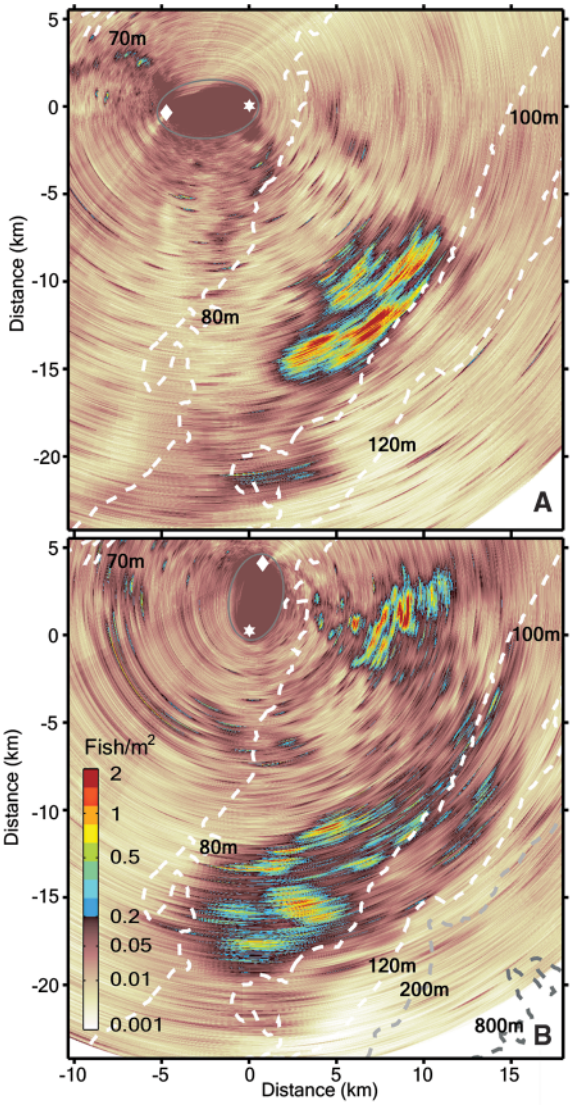

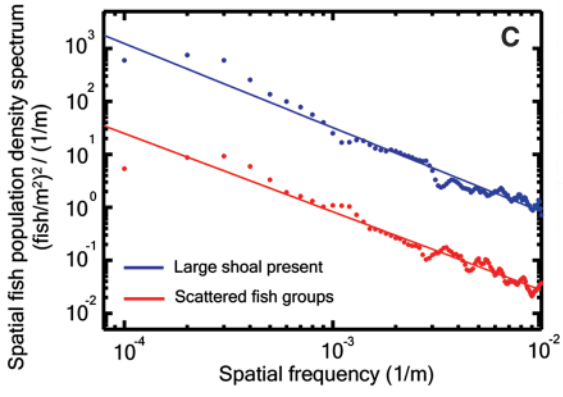

Fig. 1. Two instantaneous areal density images of fish shoals near the continental shelf edge obtained by ocean acoustic waveguide remote sensing (OAWRS) at (**A**) 09:32 EDT, 14 May 2003, and (**B**) 08:38 EDT, 15 May 2003, each acquired within 40 s. ν_A is shown in color. The moored source (the white star) is the coordinate origin in all figures at 39.0563°N, 73.0365°W. The towed horizontal receiving array (the white diamond) has 2.6° azimuthal resolution at array broadside. The range resolution is 30 m after averaging (*14*). The forward propagation of sound masks imaging inside the gray ellipse surrounding the source and receiver. The positive vertical axis points north. Depth contours are indicated by dashed lines. In (A) and (B), the continental shelf edge begins at roughly the 100-m contour. (**C**) Spatial frequency spectra, based on scores of instantaneous OAWRS images of ν_A, for cases where a large shoal is present and only small scattered fish groups are present. A consistent spectral power law of spatial frequency to the −1.5 is observed.

zontal structural characteristics, (ii) temporal evolution, and (iii) the propagation of information in very large fish shoals, containing tens of millions of fish and extending for many kilometers. All of these observations were made from distances that were typically greater than 10 km from the shoal boundaries and with sound that was at least three orders of magnitude less intense than conventional fish-finding sonar. This is possible because underwater acoustic remote sensing in the ocean (*14*–*19*) relies on the capacity of the continental shelf environment to behave as an acoustic waveguide, in which sound propagates over long ranges via trapped modes that suffer only cylindrical spreading loss rather than the spherical loss suffered in conventional fish-finding sonar technologies (*7*). The conventional approach employs only waterborne propagation paths that are restricted to much shorter ranges, on the order of the local water depth, and much higher frequencies, where attenuation is much greater (*14*).

Typical realizations of the instantaneous horizontal structure of very large fish shoals, comprising perhaps the largest massing of animals ever instantaneously imaged in nature, are shown in Fig. 1, A and B. The images are from data acquired during our May 2003 experiment (*14*) near the edge of the continental shelf 200 km south of Long Island, New York, USA. We found population centers of various size, interconnected by a network of "fish bridges" at various scales. These made the shoal shown in Fig. 1A a contiguous entity that stretched for over 10 km. A similar situation is seen in the very large southern and smaller northern shoal of Fig. 1B. All shoals exhibit large internal vacuoles and hourglass patterns previously observed only in fish groups that were many orders of magnitude smaller in area (*9*, *10*). The shoals are often very sharply bounded on the seaward side by a specific bathymetric contour of the continental shelf edge, as in Fig. 1A. This geophysical boundary apparently organizes the shoal horizontally as a social entity and may also be a navigational landmark for distant migrations (*20*, *21*). Although we found all large shoals between roughly the 80- to 100-m bathymetric contour, fish assemblages changed dramatically over time in any given region, as shown in Fig. 1 from one morning (Fig. 1A) to the next (Fig. 1B). The overall background population, for example, increases significantly from Fig. 1A to 1B, with a dense distribution of very small groups of fish appearing between the very large southern shoal and the smaller northern one. Under some circumstances, these may provide the building blocks for the fish bridges that bind a shoal together. Annual trawl surveys conducted earlier in the season and historically (*14*, *22*), as well as our visual and behavioral observations at sea, indicate that Atlantic herring, scup, hake, and black sea bass are likely species candidates in the large shoals.

The instantaneous horizontal spatial distribution of fish over wide areas follows a fractal or power-law spectral process, as quantitatively shown in Fig. 1C. Instantaneous structural similarity then exists at all scales observed, from tens of meters to tens of kilometers, and suggests that similar underlying behavioral mechanisms may be responsible for structures at all scales. This supports the qualitative argument for a fractal process in (*9*) but not the disjoint clustering of population centers that is perhaps implied there. The power law is invariant to the size of the largest fish group present, and so remains constant if an area contains a very large shoal or only much smaller scattered groups of fish, as shown in Fig. 1C. Our observations that very large shoals are structurally similar to much smaller fish groups must be a consequence of the power law. Knowledge of this power law now enables more accurate statistical predictions of the instantaneous spatial distribution of fish populations over wide areas.

Simultaneous measurements from both the conventional and the waveguide remote-sensing systems show excellent agreement in fish population density at identical time-space points along the conventional line transect (light blue line in Fig. 2, A to D), but only the waveguide technology senses two-dimensional (2D) horizontal structure and temporal change. Both systems reveal dense populations of fish at time-space points α, β, and γ, and neither system registers fish at δ beyond the shoal's seaward edge. The sharp and extensive 2D horizontal boundary of the shoal seen with the waveguide technology along the shelf edge in Figs. 1A and 2, A to D, is too transitory to be inferred from or practically measured with conventional line-transect methods, even from a series of transects. Nor can the conventional system detect or recognize the network of interconnecting bridges between population centers that waveguide technology has shown to be part of the fundamental structure of shoals. For example, the large but transitory bridge connecting the northern and southern wings of the shoal in Fig. 2, A to D, gives it a classic hourglass pattern, never previously observed over such a large scale. This is

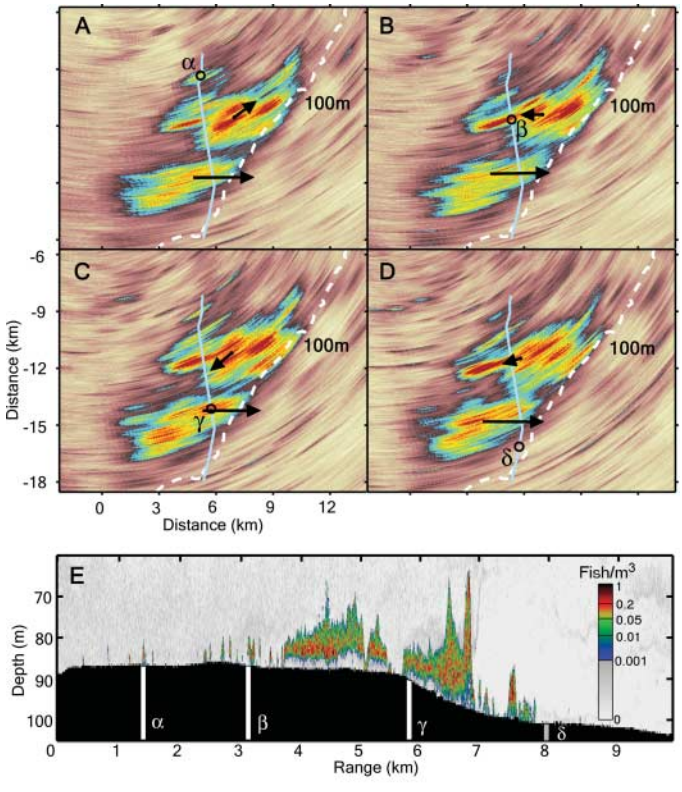

Fig. 2. A comparison of OAWRS with conventional fish-finding sonar (CFFS). (**A** to **D**) A sequence of instantaneous OAWRS areal density (fish/m^2) images taken roughly 10 min apart, starting at 11:59:05 EDT on 14 May 2003, is shown. The color bar is the same as in Fig. 1. The corresponding CFFS transect is overlain in light blue, with the CFFS position for the given OAWRS image indicated by a circle. The white dashed line is the 100-m depth contour. (**E**) Range-depth profile of fish volumetric density (fish/m^3) measured by CFFS along the transect shown in (A) to (D). White bars (in the lower black region below the sea floor) correspond to typical time-space points α, β, and γ, where both systems co-register dense fish groups [(A) to (C)]; the gray bar corresponds to point δ in (D), where neither system registers dense fish groups.

[1]Center for Ocean Science and Engineering, Department of Mechanical Engineering, Massachusetts Institute of Technology, 77 Massachusetts Avenue, Cambridge, MA 02139, USA. [2]Department of Electrical and Computer Engineering, Northeastern University, 409 Dana Research Center, Boston, MA 02115, USA. [3]Naval Research Laboratory, Stennis Space Center, MS 39529–5004, USA.

*To whom correspondence should be addressed. E-mail: makris@mit.edu

missed by the conventional line-transect method (Fig. 2E), which provides no evidence that fish in the γ group are actually well connected to those previously imaged in the β group or occasionally in the α group as well.

We noticed a daily pattern in shoal behavior that involved considerable horizontal migration and thus differed substantially from the day-to-night vertical migrations previously observed with downward-directed sonar in line transects (*23*, *24*). The pattern, observed consistently in the 3 days during which we could monitor large shoals over all daylight hours, began with the horizontal consolidation of shoals in the morning, typically organized by a sharp seaward edge extending for kilometers along a bathymetric contour of the continental shelf edge. Rapid fragmentation and dispersal followed by mid-afternoon, well before sunset when vertical migration began, as shown in Fig. 3, A to D, between 14:20 and 15:00 eastern daylight time (EDT). Fragmentation predictably began with faulting at the bridges between population centers. The bridges were apparently not sufficiently strong to withstand the internal or external pressures to diverge that acted on the shoal's internal population centers.

To describe this behavior quantitatively, time series of changing fish population (Fig. 3E) were computed at very high sample rates (50-s intervals) from imagery acquired with the waveguide technology over the hundreds of square kilometers immediately encompassing the shoal. We find that total fish population (gray curve of Fig. 3E) decomposes into the sum of a temporally stable (brown curve of Fig. 3E) and a temporally unstable (blue curve of Fig. 3E) time series. The same areal fish density (ν_A) threshold (0.2 fish/m^2) that separates the temporally stable from the unstable population is also extremely effective in spatially segmenting large shoals from smaller background groups in our instantaneous wide-area images (Figs. 1; 2, A to D; and 3, A to D). The stable component comprises the widely scattered fish groups that would form the observable background scene in the absence of a large shoal. The temporally unstable component effectively characterizes the dramatically dynamic spatial-temporal fluctuations of the large shoal. We believe that fluctuations in total population are primarily due to convergences and divergences in ν_A values above and below another threshold [minimum detectable fish density (ν_0) = 0.01 fish/m^2] where seafloor scattering mechanisms begin to become important and mask fish imaging (*15*–*19*). They may also arise from fish groups entering and leaving the survey box.

Time series enable us to introduce the concept of an autocorrelation (*25*) time scale to quantitatively characterize major temporal fluctuations in shoal population. We find that the autocorrelation time scale ranges between 5 and 10 min (fig. S1A) for the very large shoal of Figs. 1A, 2, and 3, which extends for tens of square kilometers (Fig. 3F). Shoal population (blue curve in Fig. 3E) can fluctuate dramatically in these short time scales, by 20% or a few million fish. Although dramatic, the fluctuations are consistent with the roughly 1 m/s speed at which fish in a shoal typically swim (*26*–*28*), as seen from the corresponding areal changes in Fig. 3F. The frequency spectrum of shoal population (fig. S1B) shows no remarkable periodicity, but like the spatial spectrum follows a consistent power-law process that now enables quantitative statistical predictions of

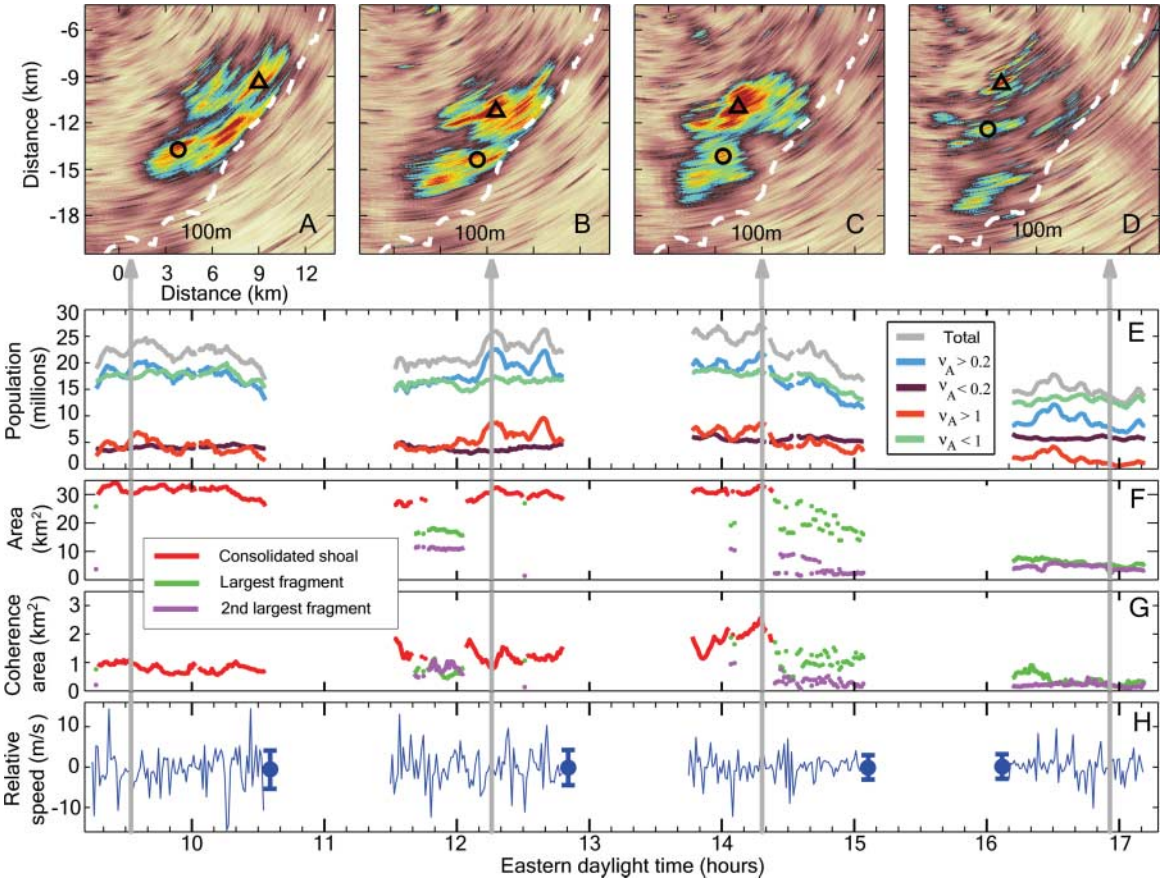

Fig. 3. Evolution of a fish shoal from morning to evening from OAWRS imagery and a time series on 14 May 2003. (**A** to **D**) Four instantaneous OAWRS images or snapshots illustrating morning consolidation and afternoon fragmentation of the shoal. The color bar is the same as in Fig. 1. Vertical arrows indicate snapshot times. (**E**) A time series of population within the area shown in (A) to (D) for ν_A within each of the thresholds specified. Gaps in the time series are due to towed-array turns. (**F**) Area occupied by a consolidated shoal or its two largest fragments for $\nu_A > \nu_{shoal} = 0.2$ fish/m^2. (**G**) The internal coherence area is the area within 1/*e* of the 2D autocorrelation peak of instantaneous OAWRS fish density within the shoal or fragment. The centroids of two particular population centers within the shoal are indicated by the circle and the triangle in (A) to (D). (**H**) Relative speeds between the centroids of the two population centers shown in (A) to (D), with mean (blue circle) and standard deviation (bars) shown for each track.

temporal behavior over wide areas and short time scales.

Shoal fragmentation and dispersal also occur very rapidly, as shown in Fig. 3E, where total population plummets in a 30-min period beginning at 14:20 EDT. More than 10 million fish disperse to below the v_0 threshold or leave the survey box. The remaining shoal fragments contain less than half the original shoal population. This and other remotely observed depopulation events were episodic, with peak dispersal rates reaching up to 0.5 million fish/min. Indeed, very large fish shoals were often lost from the view of our conventional line-transect survey system but not from the simultaneous view of our remote-sensing system based on waveguide technology.

Structural similarity can be reexamined in a time-space context by comparing time series of a shoal's outer area (Fig. 3F) to its characteristic internal area of coherence (Fig. 3G), which is the area within which population density is relatively constant. The ratio of these gives an estimate of the number of "degrees of freedom": the independent coherence cells (*25*) or primary population centers within the shoal or within its largest fragment. The fact that this ratio remains relatively constant over time even after the shoal undergoes severe fragmentation and dispersal is further evidence of structural similarity at all spatial scales, even during such dramatic events, which is consistent with fish assembly and reassembly models (*29*). Fluctuations in the shoal's outer area tend to span only a small percentage of the total area. This is true for the inner area only during periods when the shoal is not undergoing fragmentation, as can be seen in Fig. 3, F and G. Otherwise, the inner area fluctuates rapidly, reflecting an internal turbulence that probably fragments shoals.

It is remarkable that both the total population and the internal coherence area attain maxima just before the final fragmentation and dispersal of the shoal. This coincides with the shoal's transformation into a classic hourglass pattern (Fig. 3C). In hourglass patterns, migration from one wing to the other has often been observed when the depopulating wing is under attack by predators (*7*). Although we have no evidence of such an attack on the shoal in Figs. 2 and 3, and other explanations such as feeding are possible, we do see a massing of population in the northern wing of the hourglass, with a decline of population in the southern wing. This is evident in Fig. 3C and in the subsequent time series of Fig. 3F, where the largest fragment is the northern one and the second largest is the southern one.

The waveguide technology has also revealed the internal motion and migration patterns within very large fish shoals, during time spans ranging from less than 1 min to days, as shown in the imagery sequence of Fig. 2, A to D. Fundamental questions that depend on knowing "the degree of coordination in the movements" between fish populations that were previously "nearly impossible to detect" (*6*) can now be addressed. We show that even when very large shoals are highly consolidated, densely packed, and structurally similar to small groups of fish, they do not exhibit synchronized motion over short time scales, as much smaller groups often do (*10*). The many interconnected population centers within a very large shoal have centroids that undergo local positional oscillations in the horizontal, over time scales on the order of minutes, which have no correlation with each other. This is illustrated by the image sequence of Fig. 2, A to D, where velocity vectors for two centroids within the very large shoal are effectively uncorrelated in time and space.

Part of this uncorrelated internal motion arises from fish density waves occurring regularly, every few minutes, as seen by the peak events in Fig. 3H. We identify these as waves because they exceed, by an order of magnitude, the typical speed at which fish swim (*26*–*28*). Such waves travel with the apparent speed of an organized sequence of locally interconnected compaction events, like the waves that people propagate in sports stadiums by standing up and sitting down in phase, rather than at the speed at which any individual moves. The waves cause relative displacements of local population centers that are bounded by the roughly 1- to 3-km internal coherence area of Fig. 3G, as can be seen by integrating the separation rate of Fig. 3H over time. Waves have been previously seen in fish shoals spanning scales up to only tens of meters, where they have been hypothesized to provide a rapid means of communication in response to predation or other pressures (*10*, *30*, *31*). The most frequent relative motions between the local population centroids, however, occur at the much lower speeds at which individual fish can swim (fig. S1C).

Fish density waves may be used to maintain organizational coherence in very large shoals. The speed, duration, inter-arrival times, and displacements associated with the peak events in Fig. 3H suggest that waves are continuously reflecting from the boundaries of the local population center where they are confined. The waves may then provide a means for individual fish to sense the spatial extent and maintain the coherence of this local subgroup. So far, however, no evidence has appeared of communication over greater distances at a rate faster than fish can swim. Instead, we have observed substantial interaction within shoals spanning tens of kilometers by both bumping and merging of population centers, as well as by population flow across bridges. The relative slowness of this means of communication may be responsible for the inability of shoals to stay together under intense external or internal stresses.

References and Notes

1. R. A. Myers, B. Worm, *Nature* **423**, 280 (2003).
2. J. B. C. Jackson *et al.*, *Science* **293**, 629 (2001).
3. O. Sund, *Nature* **135**, 953 (1935).
4. R. Balls, *J. Cons. Perm. Int. Explor. Mer* **15**, 193 (1948).
5. D. N. MacLennan, E. J. Simmonds, *Fisheries Acoustics* (Chapman and Hall, London, ed. 2, 1992).
6. O. A. Misund, *Fish Biol. Fish.* **7**, 1 (1997).
7. H. Medwin, C. Clay, *Fundamentals of Acoustical Oceanography* (Academic Press, Boston, 1998).
8. F. Gerlotto, M. Soria, P. Fréon, *Can. J. Fish. Aquat. Sci.* **58**, 6 (1999).
9. P. Fréon, O. A. Misund, *Dynamics of Pelagic Fish Distribution and Behavior: Effects on Fisheries and Stock Assessment* (Fishing News Books, Oxford, 1999).
10. T. J. Pitcher, J. Parrish, in *The Behavior of Teleost Fishes*, T. J. Pitcher, Ed. (Chapman and Hall, London, 1993), pp. 363–439.
11. S. Mackinson, U. R. Sumaila, T. J. Pitcher, *Fish. Res.* **31**, 11 (1997).
12. D. P. Croft, J. Krause, I. D. Couzin, T. J. Pitcher, *Fish Fish.* **4**, 138 (2003).
13. W. Siebert, *Circuits, Signals, and Systems* (MIT Press, Cambridge, MA, 1986).
14. Materials and methods are available as supporting material on *Science* Online.
15. N. C. Makris, L. Avelino, R. Menis, *J. Acoust. Soc. Am.* **97**, 3547 (1995).
16. P. Ratilal *et al.*, *J. Acoust. Soc. Am.* **117**, 1977 (2005).
17. N. C. Makris, *J. Acoust. Soc. Am.* **100**, 769 (1996).
18. N. C. Makris, P. Ratilal, *J. Acoust. Soc. Am.* **109**, 909 (2001).
19. P. Ratilal, thesis, Massachusetts Institute of Technology, Cambridge, MA (2002).
20. G. A. Rose, *Nature* **366**, 458 (1993).
21. W. C. Leggett, *Annu. Rev. Ecol. Syst.* **8**, 285 (1977).
22. See www.nmfs.noaa.gov for Spring Bottom Trawl Survey.
23. V. C. Anderson, *J. Acoust. Soc. Am.* **41**, 6 (1967).
24. E. G. Barham, *Science* **151**, 1399 (1966).
25. J. W. Goodman, *Statistical Optics* (Wiley, New York, 1985).
26. I. Huse, E. Ona, *Int. Council Explor. Sea J. Mar. Sci.* **53**, 863 (1996).
27. O. A. Misund, A. Fernö, T. Pitcher, B. Totland, *Int. Council Explor. Sea J. Mar. Sci.* **55**, 58 (1998).
28. D. M. Farmer, M. V. Trevorrow, *J. Acoust. Soc. Am.* **106**, 2481 (1999).
29. T. J. Pitcher, in *Developing and Sustaining World Fisheries Resources: The State of Science and Management, Proceedings of the 2nd World Fisheries Congress*, D. A. Hancock, D. C. Smith, A. Grant, J. P. Beumer, Eds. (Commonwealth Scientific and Industrial Research Organization Publishing, Collingwood, Victoria, Australia, 1997), pp. 143–148.
30. E. Shaw, in *Development and Evolution of Behavior*, L. R. Aronson, E. Tobach, D. S. Lehrman, J. S. Rosenblatt, Eds. (Freeman, San Francisco, CA, 1970), pp. 452–480.
31. G. W. Potts, *J. Zool. London* **161**, 223 (1970).

32. This research was supported by the Office of Naval Research, the Alfred P. Sloan Foundation, and the National Oceanographic Partnership Program, and is a contribution to the Census of Marine Life.

Supporting Online Material

www.sciencemag.org/cgi/content/full/311/5761/660/DC1
Materials and Methods
Fig. S1
References and Notes

24 October 2005; accepted 4 January 2006
10.1126/science.1121756

www.sciencemag.org/cgi/content/full/311/5761/660/DC1

Supporting Online Material for

Fish Population and Behavior Revealed by Instantaneous Continental Shelf–Scale Imaging

Nicholas C. Makris,* Purnima Ratilal, Deanelle T. Symonds, Srinivasan Jagannathan, Sunwoong Lee, Redwood W. Nero

*To whom correspondence should be addressed. E-mail: makris@mit.edu

Published 3 February 2006, *Science* **311**, 660 (2006)
DOI: 10.1126/science.1121756

This PDF file includes:

Other Supporting Online Material for this manuscript includes the following:
(available at www.sciencemag.org/cgi/content/full/311/5761/660/DC1)

Materials and Methods

Our field measurements show that the areal density, dynamics, and behavior of fish populations can be continuously monitored with minute-to-minute updates over thousands of square kilometers by the use of ocean-acoustic waveguide remote sensing (OAWRS) in continental shelf-environments.

Movie S1 shows the detailed time-space behavior of fish groups in and around the large shoal during daylight hours on 14 May 2003. Frames are updated every 50 s. From 11:31:35 EDT to 12:47:25 EDT, a conventional fish finding sonar (CFFS) track is overlain including the transect illustrated in Fig. 2, A to E. A moving circle, indicating the position of the CFFS measurement, turns black when CFFS fish group density is greater than V_{shoal} and white when it is less than V_{shoal}. Co-registration of dense fish groups between the two systems is found to be high. The movie illustrates the continuous evolution of shoal morphology, from consolidation in the morning to fragmentation in the afternoon, also shown by the series of snapshots in Fig. 3, A to E. The shoal often evolves into an hourglass pattern and occasionally splits in two and rejoins before fragmentation. Small isolated fish groups are observed moving throughout the area during the day.

A waveguide is a bounded medium that efficiently channels propagating waves (*S1*). In free space, the intensity (power per unit area) of waves propagating from a point source to a distant receiver is inversely proportional to the square of the range from the source to the receiver. Source power is geometrically spread over spherical areas that increase with the square of this range. In a waveguide, spreading loss is determined by the geometry of the bounded medium. In a one-dimensional tube of constant cross-section, source power no longer spreads as range increases beyond the tube diameter, so that the mean sound intensity over the cross-section stays fixed. As a medium for acoustic waves, the ocean is bounded by the air above and the seafloor below. For ranges much greater than the ocean depth, where OAWRS is particularly useful, loss in mean intensity due to geometric spreading occurs over cylindrical areas, increasing in direct proportion to range if ocean depth is constant or nearly constant, as it typically is. Conventional fish finding sonar (CFFS) operates over ranges less than or on the order of the local ocean depth, and so is typically governed by the spherical spreading loss encountered in free-space. OAWRS also uses lower frequency waves that suffer far less attenuation from absorption and scattering (*S2*-*S5*) in the medium than the waves used by CFFS (*S6, S7*).

We have generated wide-area movies detailing the spatial-temporal dynamics of fish group behavior by concatenating sequences of OAWRS images. If the temporal sampling rate is too slow, slower than twice the rate of non-negligible spatial-temporal change (the Nyquist rate (*S8*)), a movie would appear to be aliased (*S8*) in time. This means that it would not be possible to determine all the important continuous motion over time in a scene. When aliasing occurs, motions at frequencies higher than the sampling rate become confused with low frequency motions. Examples of temporal aliasing include the discontinuous motion in viewing old movies with low frame rates, people moving in a dark room lit only by an infrequently flashing strobe light, and the illusion of slow backward or forward rotation on the spokes of a rapidly moving bicycle wheel. Similarly, sampling a spatial scene too sparsely, below the spatial Nyquist rate, leads to an inability to reconstruct its continuous spatial dependence. Our movies show no apparent signs of

spatial or temporal aliasing. This follows from spectral analysis, where, for example, the spectrum of total fish population follows a consistent decaying power law all the way to the highest frequencies (Fig. S1-B), and shows an autocorrelation time scale (Fig. S1-A) much larger than the sampling interval between OARS snapshots. The lack of aliasing follows from the fact that each wide-area OAWRS image also represents an effectively instantaneous scene (*S9*-*S11*), since the total measurement duration is shorter than the time-scale of resolvable spatial change across the scene. It takes a fish longer to swim across one of our 30-m range resolution cells (at a speed typically less than 1 m/s) than for the acoustic wave (traveling at roughly 1500 m/s) to interact with all scatterers in one of our wide area OAWRS images (roughly 30 km radius). Our overall scenes are effectively instantaneous even in the presence of fish density waves since these were highly localized in our survey area, spanning scales less than 3 km, and travel at least two orders of magnitude slower than the speed of acoustic waves (Fig. S1-C).

To form an instantaneous OAWRS image, a vertical source array sends a short broadband transmission of sound out omni-directionally in horizontal azimuth. As they travel, the sound waves reflect from the sea surface and bottom to form standing waves in depth that are called waveguide modes. These are analogous to the normal modes of a vibrating guitar string, where the entire vertical water column of the ocean acts like the plucked string. As the modes propagate horizontally outward from the source, they interact with and scatter from environmental features along the way. Scattered returns from environmental features are then continuously received by a horizontally towed line array and charted in horizontal range and bearing by temporal matched filtering and planewave beamforming (*S2, S4, S12*). The resulting image is an instantaneous snapshot of the ocean waveguide environment over the two-way travel times of the signal returns. OAWRS range resolution is fixed at the mean sound speed, c = 1475 m/s, divided by twice the signal bandwidth, or roughly 15 m before averaging. Theory, modeling, and our field measurements using calibrated targets with known positions show that ranging error of OAWRS is negligible since it is on the order of the 30 m range resolution of our image pixels after averaging, and as a consequence of modal propagation, is insensitive to the depth of scatterers or environmental features in the waveguide. OAWRS azimuthal resolution in radians varies as the acoustic wavelength λ divided by the projected array length $L\cos\theta$, where L is the full array length and the azimuth angle θ is zero at *broadside*, which is normal to the array axis. At *endfire*, parallel to the array axis, the resolution becomes roughly $\sqrt{2\lambda / L}$ radians. A sketch of our source array appears in Fig. 5 of Ref. (*S4*). Our receiving array is similar to that shown in the same figure except that it was comprised of 64-elements over a total aperture of 94.5 m. A top-down view of the bistatic measurement geometry, including the varying spatial resolution footprint of the sonar, appears in Fig. A1 of Ref. (*S13*). The beamwidth of the CFFS used in our field experiment (Fig. 2E) is 6.8°, which yields a circular 70 m^2 areal resolution footprint at 80-m depth where many of the fish groups we imaged were concentrated.

In OAWRS, the entire water column is insonified by the up-and-down going planewave components forming each waveguide mode. During our 2003 OAWRS experiment, measurements of the mean acoustic intensity after one-way transmission from the source to receiver, as well as two-way returns from the seafloor, show no sign of modal interference structure, such as peaks and nulls from coherent interference. Rather a uniform decay with range is observed, indicating a lack of modal interference, which

corresponds to a highly predictable and uniformly mixed acoustic structure over depth. This is expected for a number of reasons. Environmental scatterers such as seafloor inhomogeneities and fish are distributed randomly within the sonar resolution footprint and so decorrelate modes in the acoustic field (*S4, S14*), which then obeys circular complex Gaussian Random field (CCGRF) statistics (*S2, S9-S11, S15*), by the central limit theorem. The intensity of a CCGRF is characterized by signal-dependent noise known as speckle noise (*S9-S11*). The ocean is also active, with internal waves, eddies and turbulence. These cause small sound-speed changes in time and space that typically cause acoustic modes to decorrelate, which again leads to CCGRF fluctuations at the receiver by the central limit theorem (*S11, S15*). The one-way acoustic field measurements during our 2003 OAWRS experiment followed CCGRF statistics over time, which is consistent with the observed lack of modal interference structure in range. These observations and the consequential lack of modal interference structure in depth were verified by simulations where sound speed variations measured during our experiment were input to statistical models for waveguide propagation in the continental shelf (*S16, S17*). (Even without randomness in the medium, broadband transmissions, such as ours, also lack the delicate modal-interference nulls found in deterministic single-frequency transmission.) As a consequence of acoustic tunneling, OAWRS insonification in the upper sediment is similar to that in the water so there is no sharp boundary in the acoustic field at the water-sediment interface. In our 2003 experiment, fish shoals observed with CFFS were always found in the lower half of the watercolum, typically in layers roughly 10-m thick within meters of the seafloor, even during the dramatic population changes shown in Fig 3.

CFFS typically operates in the 20-500kHz range and measures the local depth distribution of fish at any instant by echo sounding within a narrow downward-directed beam along the line transect of a slowly moving research vessel (*S18-S21*). CFFS surveys habitats at rates in the vicinity of 0.2 km^2/hour, which are similar to those of capture-trawl vessels. Survey rates can increase by roughly an order of magnitude when standard multi-beam or side-scan technology, which also exploits local, linear, waterborne propagation paths, is used to augment CFFS (*S20, S22*). CFFS methods have provided evidence for structural similarity and been used to describe dynamic behavior in fish groups over small scales, tens to hundreds of meters (*S22-S29*). Previously, the closest to a true snapshot of the horizontal morphology and spatial distribution of a typical large shoal, of roughly 10 km length, was generated by a synthetic aperture sonar using a single horizontal source beam (*S30*). This still required roughly an hour of surveying and so was subject to significant spatial and temporal aliasing of the shoal's dynamic morphology and population. Before this, fish groups at similar ranges were observed passing through a single horizontal source-receiver beam of a specially designed fixed sonar system over time (*S31-S33*).

Both OAWRS and CFFS rely on similar principles to estimate fish population density. The former requires well-established ocean-waveguide (*S2-S4, S11, S14, S34*) rather than free-space propagation (*S7, S18-S21*) modeling of the latter. OAWRS images of areal fish population density (Figs. 1A-B, 2A-D, 3A-D) are generated by compensating for (i) two-way transmission loss in the range-dependent continental-shelf waveguide through parabolic equation modeling, (ii) the spatially varying resolution footprint of the OAWRS system, (iii) fish target strength, and (iv) source power (*S2-S4*). The OAWRS areal

population densities are consistent with those obtained from conventional fish finding sonar (CFFS) over the same time period, as can be seen by comparing Figs. 2A-D with Fig. 2E, after integrating over depth in the roughly 10-m thick fish layer of the latter. This consistency is partly because both OAWRS and CFFS population density estimates depend on the expected scattering cross section of an individual fish, which we find to have a corresponding target strength of -45 dB *re* 1m in the 390-440Hz band of our experiment based upon tens of thousands of local measurements from the conventional sonar system. (This illustrates why the most effective uses of OAWRS technology in the near future will likely be in conjunction with CFFS and direct-capture measurements.) Our empirically measured target strength, however, is also consistent with a combination of theoretical modeling (*S3*) and empirical evidence gathered by National Marine Fisheries trawl samples obtained in the same location earlier in the same season as well as historically (*S35*). Catches in the area typically consist of a variable component of Atlantic herring, scup, hake, black sea bass, dogfish, and mackerel, all of which can have target strengths within an order of magnitude of each other in the 390-440 Hz range, which is near or just below swim-bladder resonance for many of these species (*S36*).

To generate the spatial power spectrum shown in Fig. 1C, the 2-D Fourier transform of an instantaneous OAWRS areal fish density image was computed. Squared magnitudes of 2-D transforms of 10 consecutive OAWRS images, over an 8 minute period, were combined by standard periodigram averaging to obtain an estimate of the 2-D spectrum of areal population density. This estimated spectrum corresponds to the Fourier transform of the 2-D autocorrelation function of areal fish population density, normalized so that the correlation at zero-spatial lag, which is the integral of the 2-D spectrum, is the second statistical moment of areal population density. Apart from expected asymmetries arising from variations in the range and cross-range resolution of our imaging system, the resulting 2-D spectra showed uniform azimuthal dependence in wavenumber which was repeatable throughout all our observations of the shoals and scattered fish groups regardless of their orientation with respect to our measurement system. The radial-wavenumber dependence of the spectrum was then estimated by averaging within a roughly 20^{o} azimuthal wavenumber spread where the resolution of our imaging system is highest. Two periods were chosen, one at 16:19 EST of May 14 with a very large shoal present and the other at 21:30 EST of May 9 with only small scattered groups present. The 2-D spectrum was then multiplied by radial wavenumber, which is the Jacobian of the coordinate transform from Cartesian to polar, and normalized so that the 1-D integral over spatial frequency, or radial wavenumber, of either curve plotted in Fig. 1C yields the mean of the square of areal fish density over the survey area. The power laws shown in Fig. 1C were obtained by least squares fits. These results are very stable. They were repeated 4 times at uniform intervals: on May 14 from 9:34 EST to 17:02 EST, leading a mean power law of -1.55 with a 0.04 standard deviation, and on May 9, from 17:10 EST to 17:50 EST leading to a mean power law of -1.46 with a 0.03 standard deviation.

Transmission scintillation from randomness in the ocean medium due to such effects as internal waves and turbulence, and fluctuations in the received field due to source-receiver motion, and scattering from fish schools and ocean boundaries, ultimately introduce relatively little uncertainty in OAWRS images, since a standard deviation of roughly 1-dB per pixel (*S11*) is expected after our intensity averaging of the expected CCGRF measurements. (A standard deviation of less than 1-dB per pixel corresponds to

an error of less than 25% in any OAWRS intensity or areal population density estimate for the given pixel.) We applied a temporal running average window of 5-consecutive OAWRS images (250 seconds) and averaged over 2 adjacent 15-m range resolution cells to produce each image presented in Figs. 1A-B, 2A-D, 3A-D, and time series in Figs. 3E-G.

Contributions from millions of fish over hundreds of independent pixels were summed to form the population estimates of Fig. 3E. Our calculations show that fluctuations from propagation scintillation or variations in fish scattering cross-section should then lead to errors of less than 1% of the estimated value for any given temporal population sample, given the law of large numbers (*S37*).

The coherence area of Fig. 3G is the area within one e-folding length of the 2-D fish density autocorrelation function within a shoal. The coherence area is a quantitative way of describing the extent of concentrated population centers within a shoal. It is the area within which population density should not vary significantly. The decrease in coherence area in proportion with the decrease in shoal area and fish population, Fig. 3, is consistent with fish assembly and reassembly models (*S38-S40*).

The location of a population center (Figs. 3A-D) is here defined as the centroid of a local coherence area containing a population density maximum. Estimation of such a centroid involves averaging areal fish population density over a coherence area that includes roughly 30 independent range pixels. This, multiplied by the 10 independent samples from the time and range averaging used to generate each pixel, described previously, leads to μ = 300 independent samples, which reduces the speckle-noise standard deviation in fish population density to roughly $4.34/\sqrt{\mu}$ = 0.25 dB (*S10, S11*) corresponding to less than a 6% uncertainty in mean areal fish density over the coherence area. The same standard deviation and percent error is found in the mean of an equal annular area surrounding the coherence area. The image contrast, or difference in dB between the mean fish density within the coherence area and that of an equal area surrounding it, is approximately 5 dB, which is more than an order of magnitude higher than the 0.25 dB standard deviation from speckle noise. This ensures that the effect of speckle noise on our calculations of motions of mass centers is negligible. The observed horizontal separation rate, or divergence rate, of the two population centers (Fig. 3H) is consistent with the observed variations in total population (Fig. 3E), and the lower limits of OAWRS sensitivity to fish returns before seafloor scattering mechanisms become important (*S2-S4, S11, S14*).

Before adopting the fish density wave explanation, we investigated other possible causes of relative motion between population centers, all of which had to be ruled out. Effects related to the motion of our OAWRS research vessel and ocean internal waves were dismissed because these are one order of magnitude slower than the relative motions we observed between population centers. Surface gravity waves are also much slower, incoherent, and of much smaller amplitude at the time than the acoustic wavelength. We also investigated possible artifacts that could be caused by sidelobe leakage and beam merging of fish groups. We found these to be two orders of magnitude lower in speed than the observed density waves. Finally, noise from passing ships appearing as beams in OAWRS images had levels orders of magnitude lower than scattered returns from the

tracked population centers, so this mechanism was also ruled out. Most peaks shown in Fig. 3H contain multiple points leading to the apex, consistent with the coherent motion of a wave at the speeds indicated.

Fish density waves have been previously observed to propagate over meter scales, reaching maximum speeds of up to 15 m/s, in tank experiments. (*S41-S43*). These density waves could be a mechanism to signal group behavioral change similar to that described by "synchrokinesis" (*S39, S44*).

No correlation was found between OAWRS imagery and sub-bottom geologic features, after extensive investigation (*S4*).

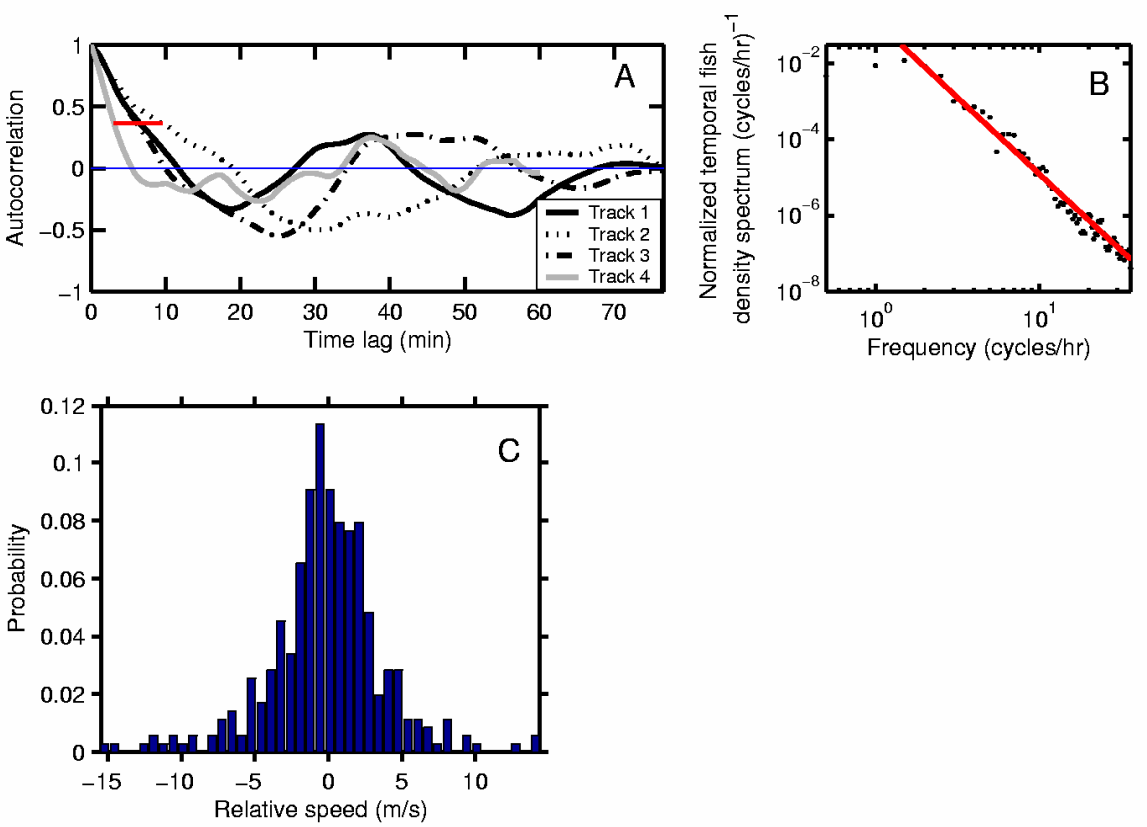

Fig. S1. (**A**) Autocorrelation functions, with red horizontal line indicating e-folding times, and (**B**) frequency power spectrum, with frequency to the -2 dependence, for the shoal population time series (blue curve in Fig. 3E). No remarkable periodicity is found. (**C**) Histogram of all relative speeds measured in Fig. 3H.

Supporting References and Notes

S1. C. B. Officer, *Introduction to the Theory of Sound Transmission* (McGraw-Hill, New York, 1958).

S2. N. C. Makris, L. Avelino, R. Menis, *J. Acoust. Soc. Am*. **97**, 3547 (1995).

S3. P. Ratilal, thesis, Massachusetts Institute of Technology (2002).

S4. P. Ratilal *et al*., *J. Acoust. Soc. Am*. **117**, 1977 (2005).

S5. C.-S. Chia *et al*., *J. Acoust. Soc. Am*. **108**, 2053 (2000).

S6. L. M. Brekhovskikh, Y. P. Lysanov, *Fundamentals of Ocean Acoustics* (Springer, New York, ed. 3, 2003).

S7. H. Medwin, C. Clay, *Fundamentals of Acoustical Oceanography* (Academic Press, Boston, 1998).

S8. W. Siebert, *Circuits, Signals, and Systems* (MIT Press, Cambridge, 1986), pp. 435-439.

S9. J. W. Goodman, *Statistical Optics* (Wiley, New York, 1985).

S10. N. C. Makris, *Opt. Lett.* **20**, 2012 (1995).

S11. N. C. Makris, *J. Acoust. Soc. Am*. **100**, 769 (1996).

S12. S. M. Kay, *Fundamentals of Statistical Signal Processing: Estimation Theory* (Prentice-Hall, Upper Saddle River, 1993), vol. 1.

S13. N. C. Makris, *J. Acoust. Soc. Am.* **106**, 2491 (1999).

S14. N. C. Makris, P. Ratilal, *J. Acoust. Soc. Am*. **109**, 909 (2001).

S15. I. Dyer, *J. Acoust. Soc. Am*. **48**, 337 (1970).

S16. Ratilal, Makris, *J. Acoust. Soc. Am.* **118**, 3532 (2005).

S17. Chen, Ratilal, Makris, *J. Acoust. Soc. Am.* **118**, 3560 (2005).

S18. O. Sund, *Nature* **135**, 953 (1935).

S19. R. Balls, *Journal du Consiel Permanent International Pour L'exploration de la Mer*. **15**, 193 (1948).

S20. O. A. Misund, *Fish Biology and Fisheries* **7**, 1 (1997).

S21. D. N. MacLennan, E. J. Simmonds, *Fisheries Acoustics* (Chapman & Hall, London, ed. 2, 1992).

S22. F. Gerlotto, M. Soria, P. Fréon, *Can. J. Fish. Aquat. Sci*. **56**, 6 (1999).

S23. H.-S. Niwa, *J. Theor. Biol*. **235**, 419 (2005).

S24. O. A. Misund, A. Fernö, T. J. Pitcher, B. Totland, *ICES J. Mar. Sci.* **55**, 58 (1998).

S25. T. J. Pitcher, O. A. Misund, A. Fernö, B. Totland, V. Melle, *ICES J. Mar. Sci.*, **53**, 449 (1996).

S26. M. T. Hafssteinson, O. A. Misund, *ICES J. Mar. Sci.*, **52**, 915 (1995).

S27. L. Nøttestad, A. Fernö, S. Mackinson, T. J. Pitcher, O. A. Misund, *ICES J. Mar. Sci.*, **59**, 393 (2002).

S28. A. Fernö *et al.*, *Sarsia* **83**, 149 (1998).

S29. F. Gerlotto, J. Paramo. *Aquat. Living Resour.* **16**, 113 (2003).

S30. J. S. M. Rusby, M. L. Somers, J. Revie, B. S. McCartney, A. R. Stubbs, *Marine Bio.* **22**, 271 (1973).

S31. D.E. Weston, J. Revie, *J. Sound Vib.*, **17**, 105 (1971).

S32. J. Revie, G. Wearden, P. D. Hocking, D. E. Weston*, J. Const. Int. Explor. Mer*. **36**, 82 (1974).

S33. D. E. Weston, H. W. Andrews, *J. Acoust. Soc. Am.* **87**, 673 (1990).

S34. N. C. Makris, *J. Acoust. Soc. Am*. **94,** 983 (1993).

S35. http://www.nmfs.noaa.gov/

S36. R. W. Nero, C. H. Thompson, J. M. Jech, *ICES J. Mar. Sci.* **61**, 323 (2004).

S37. A. W. Drake, *Fundamentals of Applied Probability Theory*, (McGraw-Hill, New York, 1967), pp. 203-216.

S38. T. J. Pitcher, *Scientia Marina*, **59**, 295 (1995).

S39. T. J. Pitcher, in *Encyclopedia of Ocean Sciences*, J. H Steele, K. K. Turekian, S. A. Thorpe, Eds. (Academic Press, London, 2001), pp. 978-987

S40. T. J. Pitcher, in *Developing and Sustaining World Fisheries Resources: The State of Science and Management, Proceedings of the 2nd World Fisheries Congress*, D. A. Hancock, D. C. Smith, A. Grant, and J. P. Beumer, Eds. (CSIRO, Collingwood, 1997), pp. 143-148.

S41. C. M. Breder, *Bull. Am. Mus. Nat. Hist.* **117**, 399 (1959)

S42. D. V. Radakov, in *Schooling in the Ecology of Fish*, D.V. Radakov, Eds. (Wiley, New York, 1973), pp.77-99.

S43. E. Shaw, in *Development and Evolution of Behavior*, L. R. Aronson, E.Tobach, D. S. Lehrman, J. S. Rosenblatt, Eds. (Freeman, San Francisco, 1970), pp. 452-480.

S44. U. Kils, thesis, Christian-Albrechts-Universität zu Kiel (1986).